48th AIAA/ASME/SAE/ASEE Joint Propulsion Conference & Exhibit
30 July - 01 August 2012, Atlanta, Georgia

AIAA 2012-3738

Capillary Extraction of the Ionic Liquid [Bmim][DCA] for Variable Flow Rate Operations

Shawn W. Miller[1] and Benjamin D. Prince[2]
Air Force Research Laboratory, Space Vehicles Directorate, Kirtland AFB, NM, 87117

Joshua L. Rovey[3]
Missouri University of Science and Technology, Rolla, MO, 65401

The ionic liquid [Bmim][DCA] is a propellant candidate in a standalone electrospray thruster or in a dual-mode propulsion system consisting of a chemical system and an electrospray system. Since limited published data exists for [Bmim][DCA], the electrospray characteristics are relatively unknown. Emission testing of the ionic liquid has been conducted to characterize the [Bmim][DCA] electrospray plume for both an external flow titanium needle and internal flow capillary. Mass spectrometric, retarding potential, and angle distribution measurements were collected for the positive polarity ions emitted from [Bmim][DCA] wetted emitters with nominal extraction voltages between ~1 kV to ~2.5 kV. The titanium needle operated at a sizably reduced liquid flow rate in comparison to the capillary. As such, only the major species of $Bmim^+([Bmim][DCA])_n$ with n=0,1 were identifiable in the quadrupole measurement range of 0-1000 amu and were formed at or near the needle potential. A typical needle angle distribution was found in these measurements. For the capillary emitter, flow rates from 0.27 nL/s to 2.18 nL/s were used to investigate corresponding alterations in the electrospray beam. The aim of the investigation was to ascertain the ability to "tune" or "dial-in" an electrospray thruster to specific ion or droplet sizes and thus specific performance levels. Unlike the limited species observed from the needle emission, the capillary measurements indicated the presence of n=0,1,2,3,4 cation species with large mass droplet contributions. The lowest flow rates indicated the highest levels of ions in the measurement range of 0-1000 amu with a mix of large mass droplets. For increasing flow rate, species < 500 amu ceased to exist leaving only the n=2,3,4 species mixed with large mass droplets in the electrospray beam. All ion species exceeded the quadrupole mass range at the upper flow rates. Ions emitted from the capillary were formed at levels below the emitter potential. Ohmic losses in the ionic liquid are likely the cause for the less energetic ions. Angular distribution measurements indicated broadening of the beam current and mass distribution for increasing flow rates.

Nomenclature

D_c	=	transport capillary inner diameter (μm)
D_n	=	capillary needle emitter inner diameter (μm)
K	=	ionic liquid electrical conductivity (S/m)
L_c	=	transport capillary length (cm)
L_n	=	capillary needle emitter length (cm)
P_0	=	reservoir pressure (Torr)
P_{VC}	=	vacuum chamber pressure (Torr)

[1] Graduate Student, Mechanical and Aerospace Engineering, 160 Toomey Hall, 400 W. 13th St, and Student Member AIAA.
[2] Research Chemist, Space Vehicles Directorate, 3550 Aberdeen Building 570, Kirtland AFB, NM 87117, and Member AIAA.
[3] Assistant Professor of Aerospace Engineering, Mechanical and Aerospace Engineering, 292D Toomey Hall, 400 W. 13th St, and Senior Member AIAA.

P_n = capillary needle emitter pressure (Torr)
q/m = specific charge (C/kg)
Q = ionic liquid volumetric flow rate (nL/s)
V_N = emitter voltage (V)
V_{Ext} = extractor plate voltage (V)
β_n = capillary length/diameter ratio coefficient
γ = ionic liquid surface tension (N/m)
ε = ionic liquid dielectric constant
μ_l = ionic liquid viscosity (cP)
ρ = ionic liquid density (kg/m^3)

I. Introduction

ELECTROSPRAY thrusters are a class of micro-electric propulsion systems that field evaporate a conductive liquid propellant. The emitted charged particles/species are electrostatically accelerated to achieve thrust. This class of thruster is ideal in operations that require precise, low thrust levels while still efficiently utilizing the stored propellant (e.g. high specific impulse). Unlike other electric propulsion systems, electrospray is discharge-free, which eliminates the risk of interference in other electrical components. As an advantage, electrospray thrusters can operate in both polarities removing the requirement for a separate neutralizer and can emit small ions and larger charged droplets. A broader specific impulse (I_{SP}) range is available in a colloid/electrospray system since the droplet size and ion/droplet ratio can be controlled.[1]

The selection of the exact propulsion system depends on the mission requirements of the spacecraft. Whether as a standalone system or in a dual-mode configuration, electrospray thrusters would fulfill the mission requirement demand for lower thrust, high I_{SP} precision maneuvering. In pairing a chemical system with electrospray for dual-mode, the ultimate benefit would be from sharing common hardware and propellant, payload mass reduction, and increased mission flexibility.[2-5] In addition, the careful selection of propellant may eliminate the need for hazardous propellants such as hydrazine.[6-9]

In earlier studies of electrospray thrusters, the propellants were salt solutions; however, now the choice propellants are molten salts known as ionic liquids (ILs). In this molten state, the cation and anion have disassociated, but the liquid overall is quasi-neutral. A subgroup known as room-temperature ionic liquids are ILs with melting points below 100 °C and are liquid at room temperature. As suggested by Fernández de la Mora, the physical properties of a IL make the use of IL advantageous for electrospray.[10] The specific properties of interest are high conductivity and negligible vapor pressure. These properties ensure that good current flow occurs between the emitter surface and the IL as well as the IL does not vaporize when exposed to a vacuum environment. In addition, the viscosity and surface tension of the liquid are important properties to note as these properties influence the flow rates and Taylor cone during electrospray operations. In the recent decade, ILs have been studied for other applications including use as explosives and rocket propellants.[8, 11] ILs have been regarded as benign, but recent work highlights that many ILs are combustible when approaching the decomposition temperature.[12-14] Given these new results, ILs have a future in both chemical and electric propulsion.[15] Determining ILs that possess properties conducive to both forms of propulsion can result of a common propellant in a dual-mode configuration.

Table 1. Bmim-DCA cation species and associated masses for < 1000 amu.

n Value	Cation	Mass (amu)
0	$Bmim^+$	139
1	$Bmim^+([Bmim][DCA])$	344
2	$Bmim^+([Bmim][DCA])_2$	549
3	$Bmim^+([Bmim][DCA])_3$	754
4	$Bmim^+([Bmim][DCA])_4$	959

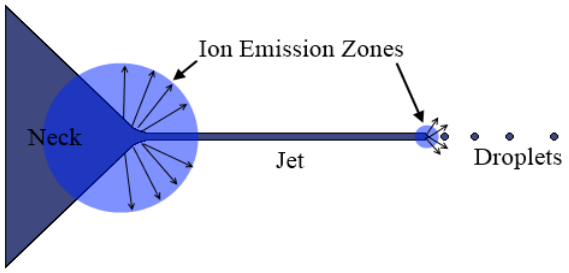

Figure 1. Taylor cone structure and ion emission zones.

The common IL frequently used in electrospray studies has been [Emim][Im] (1-ethyl-3-methylimidazolium bis(trifluromethylsulfonyl)imide). This IL has good conductivity and viscosity properties allowing for excellent electrospray performance. However, [Emim][Im] does not possess the fundamental combustion properties that would permit the liquid to be utilized in a chemical propulsion system. The lack of oxidizer in this IL and difficulty

to ignite contribute to [Emim][Im] rejection as a candidate propellant in chemical propulsion.[16] [Bmim][DCA] (1-butyl-3-methylimidazolium dicyanamide) is an IL exhibiting similar physical properties to [Emim][Im] suggesting that electrospraying of [Bmim][DCA] could be possible. Though not as extensively studied as [Emim][Im] in the electrospray thruster application, [Bmim][DCA] is beginning to be investigated. The potential use of the [Bmim][DCA] IL in chemical engine applications has been studied previously and has been found to be hypergolic with standard storable oxidizers.[3] In fact, [Bmim][DCA] exhibits a heat of formation value double that of hydrazine (206.2 kJ/mol and 109.3 kJ/mol respectively).[16] The heat of formation is significant in combustion since it is used to estimate equilibrium composition and chemical performance such as I_{SP}. A higher heat of formation value corresponds to an increase in energy released upon combustion.[16] Based on these facts, [Bmim][DCA] is a potential propellant candidate for both types of propulsion systems. Table 1 lists the relevant cation species of [Bmim][DCA] for the study to follow.

The physical phenomenon responsible for the usefulness of ILs in electrospray thrusters is the formation of the Taylor cone structure (see Fig. 1). The IL either flows down the capillary or along the emitter surface depending on the style of emitter. In the presence of a high electric field, the IL flows along the emitter to the tip. At the tip, the flowing IL forms a Taylor Cone which results from the balance between the pull of the surface tension of the liquid and the pull of the applied electric field (see Fig. 1). Fernández de la Mora and Loscertales determined the proportionality between the conducting liquid parameters and the emitted current. This proportionality can be seen in Eq. (1) where the specific charge has been related to the conducting liquid parameters. In this equation, the specific charge is proportional to the conductivity and surface tension, but inversely to the volumetric flow rate and density.[1, 17, 18] As a result, the thrust and I_{sp} can be adjusted by variation in the parameters. A lower specific charge will result in an increased thrust while a higher specific charge will result in an increased I_{sp} (efficient propellant usage). Of the variables in Eq. (1), the volumetric flow rate is the most readily adjustable parameter due to independence from IL properties or system design. Adjustment is made by changing the backing pressure on the IL source. Conductivity, density, surface tension, and dielectric constant are a function of the IL used and temperature. Further adjustment to the specific charge is made by changing the IL and temperature, though not as easily changed as the flow rate.

$$\frac{q}{m} \propto \frac{1}{\rho}\left(\frac{\gamma K}{\varepsilon Q}\right) \tag{1}$$

This study focuses on emitting the IL [Bmim][DCA] from two different types of emitters; an external flow titanium needle and an internal flow capillary. The emission testing has been conducted to characterize the [Bmim][DCA] electrospray plume. For the capillary emitter, a variable IL volumetric flow rate range has been used to establish possible alterations to electrospray plume composition. An angle-resolved quadrupole mass spectrometric analysis has been used to collect mass spectrometric, retarding potential, and angle distribution for the positive polarity [Bmim][DCA] ions (i.e. cations). The aim of the investigation has been to ascertain the ability to "tune" or "dial-in" an electrospray thruster to specific ion or droplet sizes and thus specific performance levels.

II. Experimental

A. Apparatus

Figure 2 is a schematic diagram of the experimental setup used for the angle-resolved quadrupole mass spectrometric analysis.[19, 20] The setup consists of three sections: rotating emission source, near-field targets, and far-field targets. The rotating emission source is a framework affixed to a rotating axis (z-axis) that is perpendicular to the thrust beam axis (x-axis). This rotation allows for the selection of the desired angle of the electrospray beam for angularly resolved measurements. The framework supports the electrified extractor plate and electrospray emitter

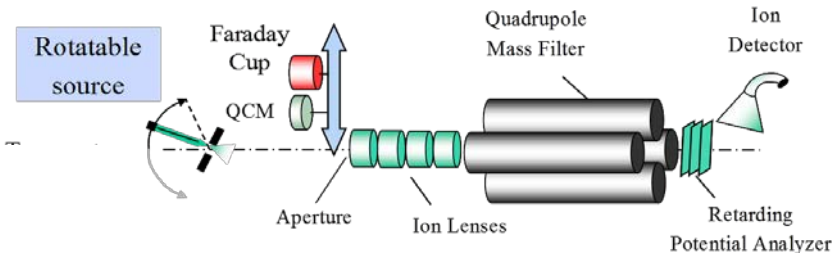

Figure 2. Colloid thruster experimental setup.

(e.g. etched metal needle or capillary needle). The electrospray emitter is positioned roughly 1 mm to 2mm from the extractor orifice. This 1.5 mm or 3 mm diameter orifice allows for the passage of the electrospray plume. Typical turn-on extraction voltages range from 1.1 kV to 2.2 kV in a DC voltage mode depending on the IL and electrospray emitter used. An AC voltage mode can be applied as well if AC data collection is desired. In the angle-resolved measurements, no focusing lenses are used to focus the electrospray beam. The extractor electrode is the sole source of particle acceleration.

The first set of targets downstream of the emission source is the near-field targets. These targets are mounted on a translating z-stage. They consist of a Faraday cup, quartz crystal microbalance (QCM) (XTM/2, Inficon), and a cylindrical lens element. The Faraday cup and QCM allow for the measurement of current and mass flow rate of the electrospray beam respectively. Equally sized apertures (6 mm diameter) are used on both targets. With the use of the rotatable emission source, the near-field targets are ~ 18 mm from the source. When the cylindrical lens element is moved into the electrospray beam path, the element allows for the passage of the beam further down the instrument to the far-field targets.

In the far-field are the quadrupole mass filter with a set of focusing lenses at the entrance, a set of three grids used for the retarding potential analysis (RPA), and an off-axis channeltron detector. The far-field targets start at a distance of ~58 mm from the emission source. The filter, grids, and channeltron can be configured for electrospray beams of either ion polarity.

B. Charged Emission Sources

For the work to be discussed, two different types of electrospray emitter sources were used in the data collection. These two emitters along with the extractor are featured in Fig. 3 and represent the most widely used types of emitters. The difference between the two emitters is the paths in which the electrospray fluid, in this case the IL, is transported to the tip. For the etched metal needle, the IL is transported along the external surface of the needle and extraction is solely dependent on the electric field to induce a flow. The capillary needle has an internal flow of IL that is dependent on a backing pressure of the fluid feed system. Higher flow rates can be achieved using a capillary needle than with a metal needle.

1. External Flow: Etched Metal Needle

Initial study of the IL was conducted using a metal needle. The needles used in this data collection were composed of a 20 mm diameter titanium wire which was modified by an electrochemical etching process to produce a sharp tip. This process resulted in a tip with a radius of curvature of approximately 20μm. A short piece of 10 mm diameter titanium wire is spot welded ~3 mm from the tip. This junction forms a reservoir location for a drop of IL to flow from during operation. The IL drop was applied externally to this point and then placed into high vacuum with no further processing.

2. Internal Flow: Capillary Needle

The second type of emitter used was a capillary. This emission source is more complex than the metal needle. IL is fed by a fluid feed system from a reservoir, through a transport capillary, and out the tip of the "thruster" capillary. In the data set to follow, the transport capillary was a fused silica capillary of 100μm inner diameter and 82.5 cm in length. The thruster capillary was a stainless steel tapered tip capillary of 50mm inner diameter and of 3.5 cm length. Both were supplied by New Objective. The two capillaries were connected using a capillary union (Upchurch Scientific). The flow rate of IL propellant through the capillaries is regulated by maintaining a

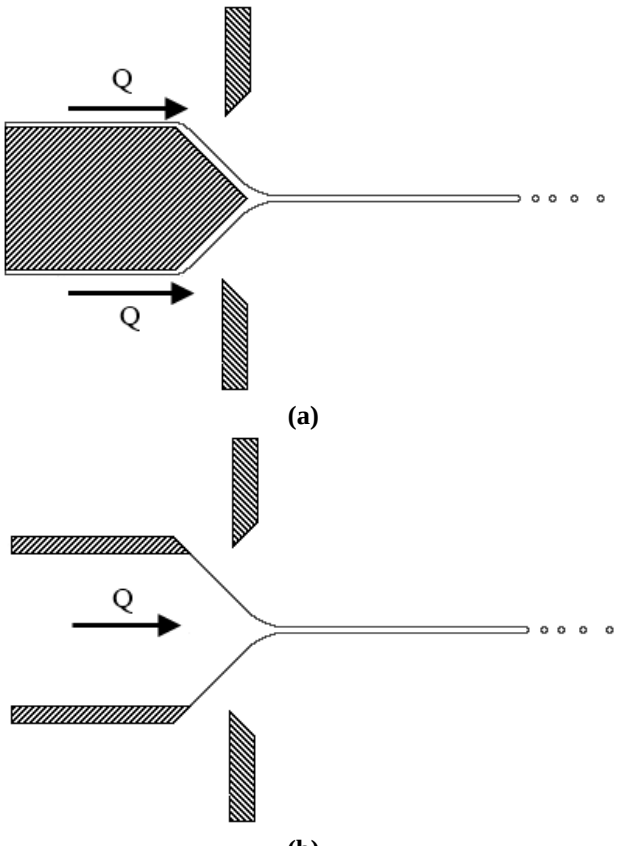

Figure 3. Two types of electrospray emitters, (a) external flow metal needle; (b) internal flow capillary needle.

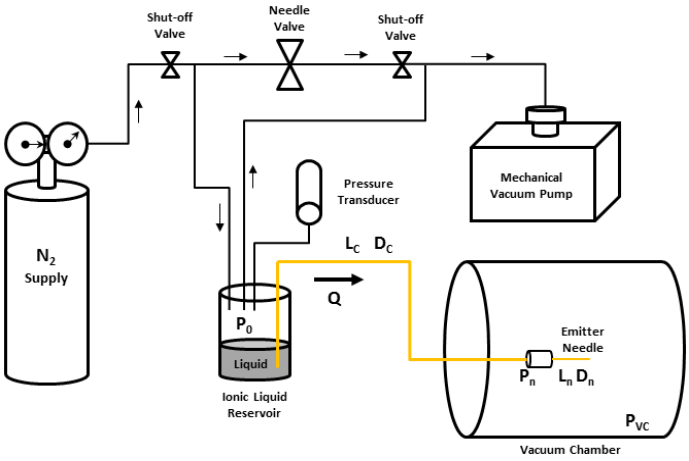

Figure 4. Capillary fluid feed system. Capillary supply and emitter indicated by orange path. Arrows indicate flow path of gas.

constant pressure of nitrogen in the propellant reservoir, which will be further discussed next.

3. Fluid Feed System

Figure 4 illustrates the fluid feed system used with the capillary needle. As can be seen, the reservoir pressure P_0 provides a backing pressure on the IL. This constant pressure is maintained by admittance of an inert gas, in this case nitrogen, into the reservoir and by pumping with a mechanical pump. The needle valve allows for direct control and setting of the reservoir pressure. This feed system is similar to the system used by Lozano[21], but the direct monitoring of the reservoir pressure using a pressure transducer (MKS) eliminates the need to calculate the reservoir pressure based on the regulated source gas or pumping speed of the mechanical vacuum pump. This control allows for smaller pressure increments to be used with an instant reading of P_0. When not in use, the ionic liquid reservoir remains under rough vacuum (<100 mTorr) to ensure no water absorption that could affect capillary flows.

The flow rate through the capillary setup is measured using the bubble method. A bubble of nitrogen is introduced into the capillary and the velocity of the bubble traveling in the capillary is measured using a visual magnifier. For the data collected, the velocity was measured in the transport capillary, external of the vacuum chamber.

III. Results and Discussion

A. Needle Emitter

Figure 5 is a plot of both angularly-resolved current density and mass flow rate. Max readings of 2.2 nA/mm^2 and 21.8 ng/s respectively occur at the centerline of emission at 0°. The current density occurs over a broader range of angles than the mass flow rate suggesting that most contributing mass flow occurs within 15°-20° of the centerline. At angles greater than 20°, negative mass flow is recorded indicating that ions are removing material from the surface of the quartz crystal. The current density at the widest angles is due to low mass, fast moving ions. This particular needle emitter shows good symmetry about the centerline axis. Data were collected from ~ ±35° for all measurements of the needle emitter plume. The average *m/q* of the metal needle spray, as estimated from the Faraday cup and QCM measurements, is ~19,300 amu. The total emission current of the needle plume was ~200 nA.

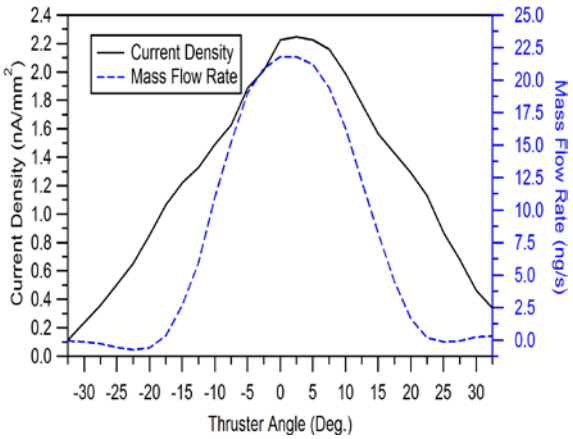

Figure 5. Needle current density profile and mass flow rate generated at each thruster position angle.

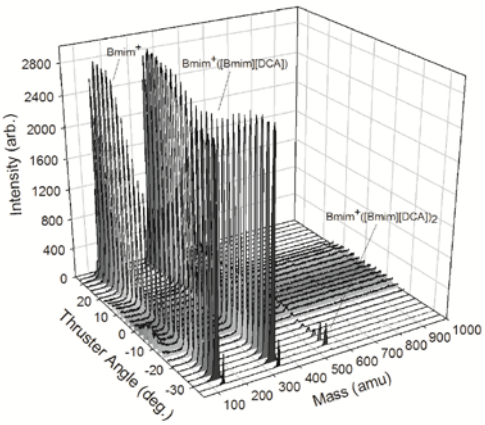

Figure 6. Cation mass spectrum of [Bmim][DCA] for a needle emitter.

Figure 6 illustrates the angle-resolved mass spectrum of [Bmim][DCA] from a needle emitter. For this low IL flow rate, only low mass cations are detectable with the mass filter. The monomer and dimer cations are the only emission products of [Bmim][DCA] that occur with significant intensities. Trace amounts of the $Bmim^+([Bmim][DCA])_n$ for n=2 and n=3 can be identified in the spectrum particularly in the baseline reading near the centerline. The low intensities inhibit the acquisition of high-quality RPA data and indicate these species are not significant contributors to the electrospray beam. Only at large angles does the n=2 cation have sufficient intensity to be measurable in the RPA scans. The elevated baseline reading between ±15°, which has been observed previously in needle mass spectra, is attributed to large *m/q* species that are not completely filtered out by the mass filter and reach the detector.[22, 23] It is possible to use the intensity trend of each species to approximate the location of origin of that species in the Taylor cone. Maximum n = 0 cation intensities are observed at high angle values. This distribution is expected when ions originate from the neck of the Taylor cone as opposed to the jet since the jet is expected along the centerline axis. Energy measurements obtained with the RPA and presented next will aid in further identifying the origination of these ions.

Figure 7 shows the energy distributions of ions emitted from the needle emitter for the on-axis and off-axis cases. The energy distributions are obtained by using the derivative of the processed retarding potential data. The retarding energy potential for each mass consists of smoothed, averaged data of five RPA scans. A smoothing process, consisting of a five point boxcar smoothing, is used to minimize noise in the data scans. The on-axis case of Fig. 7A reviews three cations with *m/q* values of 139 amu, 344 amu, and >1000 amu. For all three, peak energy is slightly less than 500 eV (emitter bias potential). Given the slightly lower potential, the most likely source of these ions is from the jet emission zone. Compared to the neck region, the jet extends into the electric field and undergoes potential drops due to the resistance differences of the liquid and needle (Ohmic losses). The baseline observed between ±15° (Fig. 6) indicates that charged droplets (*m/q* >1000 amu) are being emitted on-axis with significantly lower (and broader) energies consistent with emission at the end of the jet region.

The off-axis data of Fig. 7B show different trends than those observed for the on-axis data. The peak of the energy distribution is centered at or slightly higher than 500 eV which suggests cation origination near the emitter. The only emission zone near a potential of 500 V is the neck region. The 549 amu cation energy distribution was

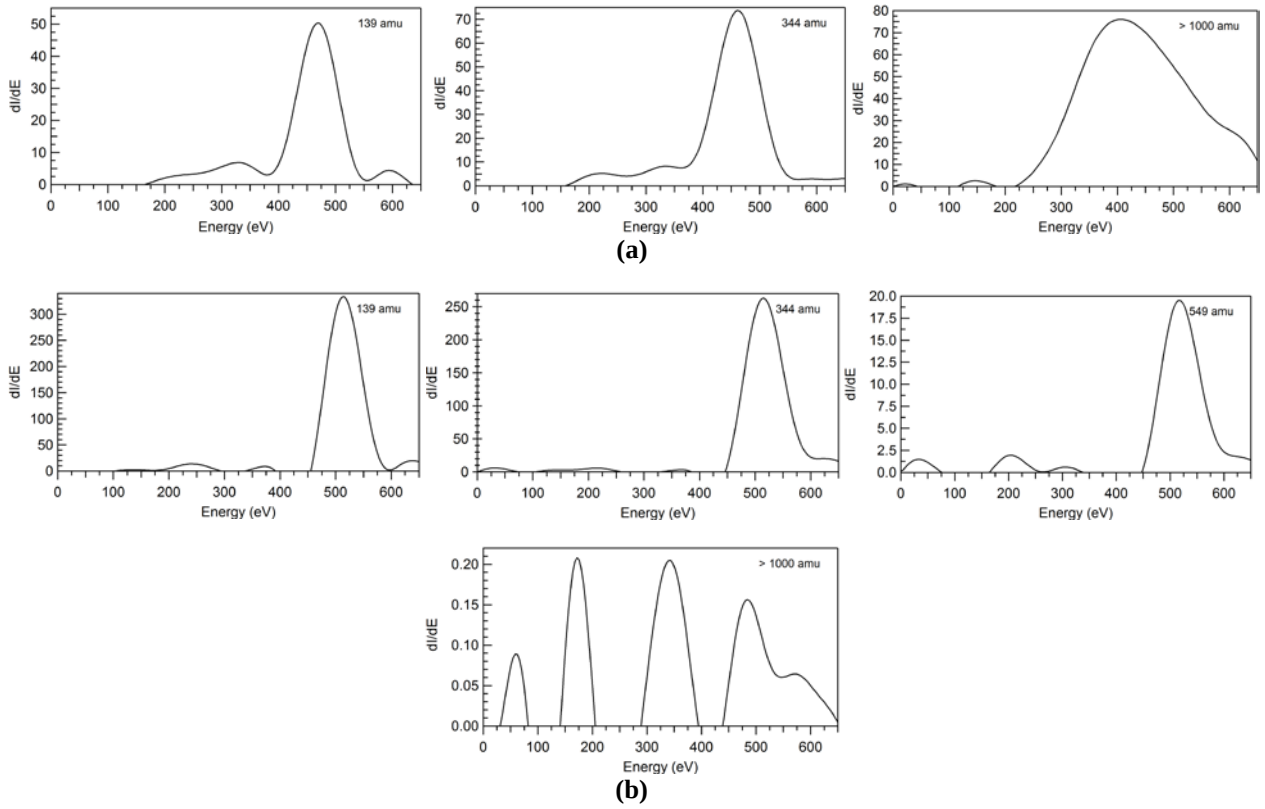

Figure 7. Retarding potential analysis of the needle emitter plume, (a) On-axis (i.e. 0°); (b) Off-axis (i.e. 27.5°) for 139 amu, 344 amu, 549 amu, and *m/q* > 1000 amu. For the on-axis, 549 amu case, no significant results were obtained and as such this can was omitted.

only detectable in the RPA for the off-axis. These ions were found to have energies similar to the other low mass ions with potentials near 500 eV. This finding indicates that all three species emit from the same location at the neck of the Taylor cone very near the emitter tip. The absence of any real structure in the > 1000 amu mass indicates that droplets do not occur at these high angles.

B. Capillary Emitter

The remaining sections pertain to the electrospray results obtained from a capillary emitter configuration. In addition to plume analysis results of current density, mass flow rate, mass spectra, and retarding potential analysis, ionic liquid flow rate calibration data are also presented. The capillary emitter data will be presented in terms of variable flow rates extending from 0.27 nL/s to 2.18 nL/s.

1. Flow Rate Calibration

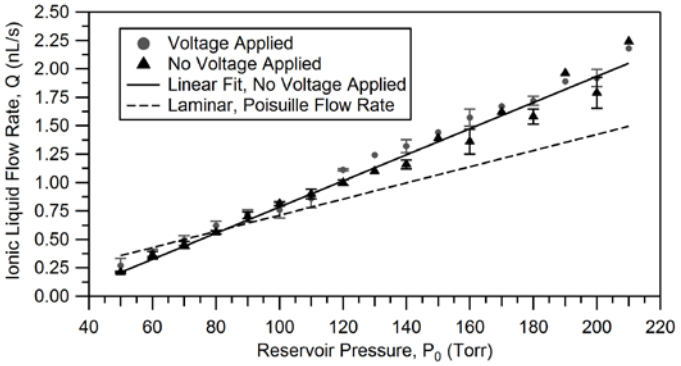

Figure 8. Comparison of experimentally determined and theory based flow rates vs. reservoir pressure, P_0.

Ionic liquid volumetric flow rate is used to compare plume data for various reservoir pressures of P_0. This is done to achieve data independence from the experimental setup. P_0 is dependent on the nitrogen supply pressure, vacuum pumping speed, and length of gas transport lines. By providing the volumetric flow rates, any independent comparisons can be conducted by only alternating the capillaries dimensions and reservoir pressure as needed in Eq. (2). As specified earlier, the bubble method is used to determine the IL flow rate in the capillary.

The ideal volumetric flow rate (laminar, Poiseuille) can be determined using Eq. (2) for Q and Eq. (3) and Eq. (4) for required variables. Note that Eq. (2) can be used for the transport capillary or the capillary needle emitter as the flow rate between the two must be equivalent by conservation of mass. In Fig. 8, the ideal flow rate is compared with measured flow rate for two conditions: voltage applied for the establishment of an electric field and no voltage applied. Data for these two conditions were collected to determine if any flow rate could be attributed to the presence of the electric field. As can be seen by the linear fit, the two experimental data sets share a similar linear trend. Within each data set, specific pressures were selected to have multiple flow rates values collected. The average values with a standard deviation are shown in Fig. 8 in those cases. The overlap in the two data sets at these points suggests good agreement for the experiment. Based on the trend and correlation between data points, the presence of the electric field appears not to influence the IL volumetric flow rate as measured in the transport capillary.

$$Q = \frac{\pi D_c^4}{128\mu_l}\frac{\left(P_0 - P_n\right)}{L_c} = \frac{\pi D_n^4}{128\mu_l}\frac{\left(P_n - P_{VC}\right)}{L_n} \tag{2}$$

$$P_n = \frac{P_{VC} + \beta_n P_0}{1+\beta_n} \tag{3}$$

$$\beta_n = \frac{L_n}{L_c}\left(\frac{D_c}{D_n}\right)^4 \tag{4}$$

There appears to be significant disagreement between the experimental data and the ideal volumetric flow rate. If the trend for the experimental data were extrapolated to 0.0 nL/s, the minimum pressure obtained would be ~30 Torr, not 0 Torr as in the ideal case. Other studies have shown Eq. (1) accurately models the flow rate. In fact, Lozano showed clear correlation between experimental and ideal values for capillary emission of the IL [Emim][Im].[21] Two possible reasons can be given to explain the discrepancy. The choice of IL viscosity value is one possible source of error. Limited data exist on the physical properties of [Bmim][DCA] and current viscosity data are only available from Carvalho[24] and Sanchez.[25] The two independent sources report 39.1 cP and 33.2 cP

respectively. The viscosity value used to calculate the ideal flow rate trend in Fig. 8 was 33.2 cP. A larger viscosity value will result in a more gradual slope for the flow rate trend. For comparison, the viscosity value was varied in Eq. (2) and ~20 cP to ~25 cP provided the best fit to the experimental data albeit with an offset occurring so that the ideal case's y-intercept remains at 0.0 nL/s. A viscosity within that range, while low, is within the neighborhood of the two established viscosity values and still justifiable if chosen to be used. In both studies, the ionic liquid was under vacuum before measurements were taken to eliminate any water absorption that may affect the physical property data values.

The second possible influence was the introduction of the bubble into the flow for flow rate measurement. Two sets of bubbles (~4 bubbles per set) were introduced into the flow at a P_0 of 100 Torr to allow for rapid, continuous measurement of flow rates without adding extra delay waiting for a bubble to arrive at the velocity measurement point. Between the flow rate measuring point and the reservoir, the capillary is not viewable for ~ 5 in. As a result of the method for bubble generation, the bubble would be at 100 Torr while the backing pressure (P_0) could vary between 50 Torr and 210 Torr to correspondingly change the flow rate. The bubble would in fact expand and contract accordingly to the applied backing pressure. As a result of the pressure differential, error could have been introduced into the flow rate data causing the offset in y-intercept and change in slope of the experimental data. Additional analysis is required to determine the importance of this effect. This will be done using bubbles with corresponding pressures as the reservoir pressure.

2. Plume Analysis

The plume analysis was conducted for a capillary needle emitter and extractor set to a total extraction voltage of 2.2 kV (+500 V_N, -1700 V_{Ext}). Given space limitations between the detectors and the rotatable source, angular measurements were possible only between ± 30°. Note that for the figures on current density, mass flow rate, and mass spectra, the collected data were mirrored about 0°. The data sets were only collected for -30° to 0° and as such the illustration of full angular trends of the data is artificial. Based on previous needle experiments plume symmetry about the centerline is a reasonable assumption. Some variations in symmetry does occur for needle emitters as seen with the needle emitter data reported here, but that can be attributed to the shape and surface etching process. Capillaries are better uniformly shaped in manufacturing. Further data collections will be conducted to verify this assumption. For a desired plume property, the data were collected at a particular angle with the flow rate being varied between 0.27 nL/s to 2.18 nL/s.

Figure 9 illustrates the variation in the current density profile as a function of flow rate. The striking aspect of the current density data is that the current profile widens for increasing flow rate. This suggests that current is in fact broadening across the thrust beam. This may mean that the charged particles (ions, drops, etc.) may be occurring in different concentrations for a given angle as a function of flow rate or that the composition of the beam in totality is shifting from ions dominate to being more charged droplet dominate. The maximum current density of 2.04 nA/mm^2 is obtained at 0° (on-axis), flow rate of 0.27 nL/s.

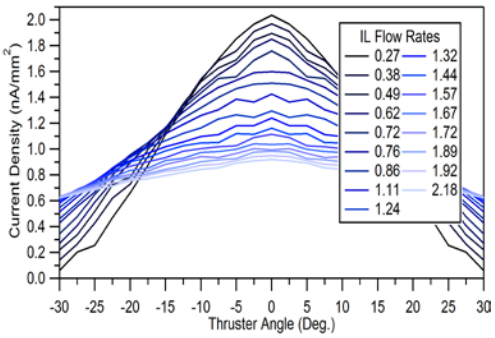

Figure 9. Capillary plume current density profile. Current density vs. thruster angle for discrete IL flow rates.

Figure 10 illustrates that even at low flow rates, the capillary emits significantly greater mass than the needle emitter. Besides the flow rate at 0.27 nL/s, data were collected at a limited number of points to prolong accurate results from the QCM. Since [Bmim][DCA] has a low vapor pressure and does not vaporize under vacuum, any substantial amount of liquid released will collect on the surface of the QCM. Based on the behavior of the QCM while working with a capillary source, the mass flow emitted was substantial enough to affect the reading, particularly above 100 ng/s. By observing the quartz crystal frequency during high IL flow rates, it was noted that a substantial drop in crystal frequency occurred. When the drop in frequency occurred, the mass flow rate reading correspondingly dropped. During the frequency changes, the discrete mass flow rate data points no longer maintained an identifiable trend. Viewing the crystal after the frequency change revealed a significant deposit of IL on the

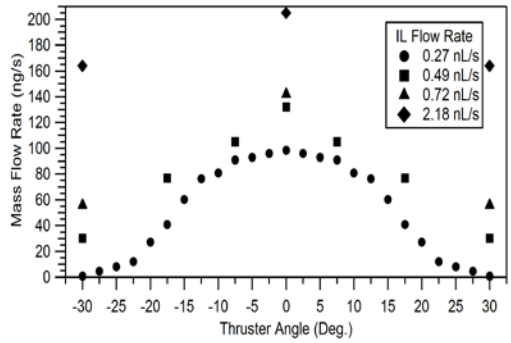

Figure 10. Mass flow rate vs. thruster for various IL flow rates.

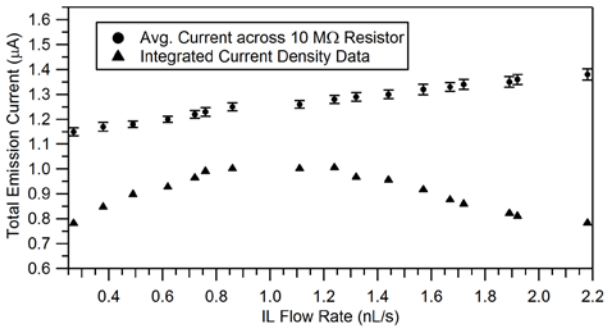

Figure 11. Total emission current as a function of IL flow rate.

crystal. Cleaning the crystal of the IL deposit restored the QCM reading until the IL built up again. Ultimately, the QCM measurements had no correlation because the crystal frequency had been altered by the IL presence. The thin film deposition assumption was violated by amount of IL deposited on the crystal's surface. Consistent, repeatable results were only obtainable when the IL deposit layer was not significant. This failure was not observed with the use of needle emitters and the crystal frequency did not rapidly decrease as had been observed with the capillary.[20, 26] The available data, at the lowest flow rates, does indicate a typical bell shaped trend peaking at 0° and ultimately increasing in value as flow rate increases. Interestingly, the data do not indicate any regions of ion sputtering (negative mass flow) on the crystal surface. Negative mass flow at high angles with needle emitters has been ascribed to the sputtering (mass removal) of high kinetic energy ions and the absence of larger species (such as that seen in Fig. 6). This suggests, in the capillary case, that either such ions are not present in the beam at high angles, significant larger masses are being emitted masking the results of sputtering, or that the kinetic energies of the emitted species are not sufficient to induce sputtering. Given the broadening seen in the current density profile and low flow rate QCM values as a function of flow rate, larger masses are likely present in the beam at high angles. The maximum mass flow at 0.27 nL/s was 98.4 ng/s. The average *m/q* of the capillary at 0.27 nL/s was 165,000 amu determined from the available QCM and Faraday cup data.

Figure 11 shows the total emission current determined by two different methods. The average current data is obtained by measuring the potential across a 10 MΩ resistor on the emitter voltage line. By application of Ohm's law the total emission current can be obtained. For this emitter, the total emission current is around 1.1 μA to 1.4 μA. The associated error bars represent the standard deviation of the data set. The total emission current was also calculated by integration of the current density profile as conducted by Manzella.[27] However, unlike Manzella where there was a ~20:1 ratio between detector separator distance to detector aperture size, the ratio was ~3:1 for the current experimental setup. These data were then integrated similar to Manzella to obtain the total emission current at each flow rate. As can be seen, there is some variation in the values of the two methods of determining emission current. As the flow rate increases, the difference between the two methods increases. This is indicative of the broadening of the current seen in Fig. 9 where the distribution of current is clearly broadening as flow rate is increased. At 2.18 nL/s, the maximum current density at 0^o is approximately 0.9 nA/mm^2 while at 30^o has only decreased to 0.6 nA/mm^2.

Figure 12 illustrates the angular-resolved mass spectra for [Bmim][DCA] at three selected volumetric flow rates; 0.27 nL/s, 1.24 nL/s, and 2.18 nL/s. Two different intensity scales are shown since at high volumetric flow rates the identifiable ions occur at a reduced intensity. For all capillary mass spectra data, the same voltage settings were used on the channeltron detector. By doing so, a relative comparison between the data sets of each flow rate can be conducted. Settings were not the same between capillary and needle spectra measurements. No relative intensity comparison can be made between the two emitter data sets. For the capillary mass spectra, all cation species in the quadrupole mass range $(Bmim^+([Bmim][DCA])_n$ for n=0,1,2,3,4) are present in the mass spectra; though under increasing flow rate conditions the intensity of the species decrease. Cation species less than 500 amu only occur in faint amounts at higher flow rates. The intensity levels for cation species greater than 500 amu underwent a change for increasing flow rate as well. The intensity change resulted in a centerline max distribution to a uniform distribution appearance across all angles for species greater than 500 amu. This suggests a broadening of the given ion species for increasing flow rate and matches the changes seen in the current density and mass flow rate as volumetric flow rate increased. The three illustrations capture the transitional aspect of the mass composition of the beam. It is clear that the 0.27 nL/s flow rate highlights the beginnings of more needle-like emission. If the IL flow rate was further reduced, a supposition on the mass spectrum appearance would be a gradual transition to reflect needle emitter spectrum. In such a transition, all cations for n>2 would cease to be detected in the spectrum.

The capillary spectrum obtained at the lowest mass flow rate has a narrower angular spread than that observed for the needle emitter. The lowest flow rate maintains the similar ion angular distribution at higher angles to that of the needle with ions peaking at ~20° in the needle and ~10° for the capillary. As the flow rate increases, the distribution is clearly centered about 0° and appears nearly flat at the highest flow rates. At 2.18 nL/s, only the smallest intensities are observed for masses less than 1000 amu. The most likely explanation is that the beam

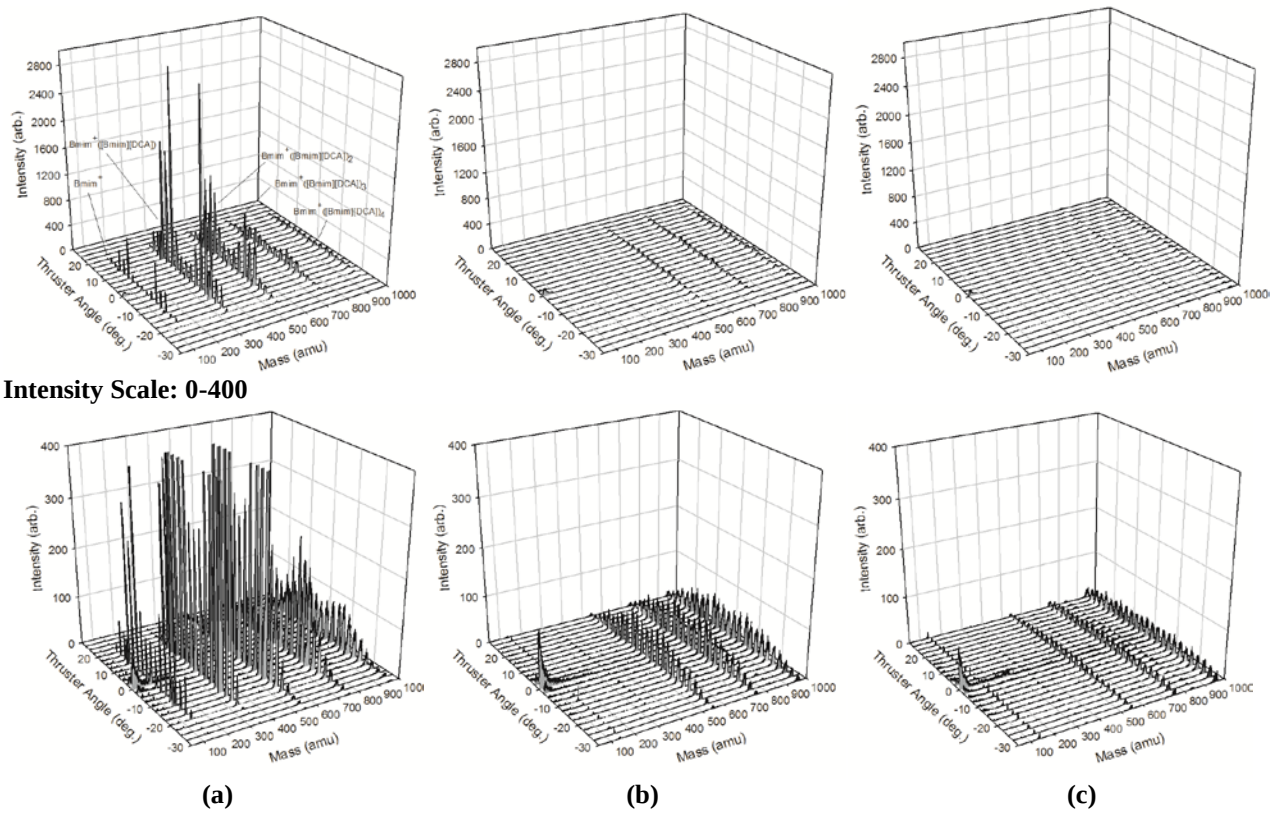

Figure 12. Capillary emitter angle-resolved cation mass spectra for IL flow rates at, (a) 0.27 nL/s; (b) 1.24 nL/s; (c) 2.18 nL/s.

composition has transitioned to larger charged masses (i.e. droplets) as flow rate increases. The baseline observed along the centerline in the needle data is absent in the capillary spectra at all flow rates.

Figure 13 and Figure 14 are the energy distribution data for 0.27 nL/s and 1.24 nL/s respectively at two different angles (0° and 15°). The distribution for 2.18 nL/s was not included since the mass spectra showed weak intensity of the cation masses and the 1.24 nL/s data were sufficient to explain the events at higher flow rates. In conducting the retarding energy potential scans, four masses were selected to "sample" at each angle and flow rate. These masses were 344 amu, 754 amu, 800 amu, and m/q > 1000 amu. The first two masses represent cations at the low and high end of the mass filter range. The 800 amu was scanned for any background that may mask or offset the actual RPA data and must be subtracted from the measurements at the cations. For m/q > 1000 amu, this is an all pass scan, which allows for any mass greater than 1000 amu pass through the mass filter and into the RPA grids. The result is an energy scan of the larger masses that exist in the electrospray plume, but not detected in the earlier mass spectrometric scans. Note that the energy distribution data in Fig. 13 and Fig. 14 were not processed as thoroughly as the data in Fig. 7.

In Fig. 13, the energy distributions for each cation species (344 amu, 754 amu, and m/q >1000 amu) illustrate similar trends for both the on and off-axis data although the peak energies shift slightly to higher values as the thruster angle increases. The shift in energy peak is not surprising for the 0.27 nL/s case due to the similar angular distribution of the small ions for both the needle and capillary. The low mass ions, at this flow rate, contribute more to the beam composition at higher thruster angles. The most surprising difference is that peak energy of all sampled species, even those of the lower mass species, are well below that of 500 eV as seen in the needle data.[19, 28] For both needle and capillary emitters, a bias potential of 500 V was used. In needle emitters, most ions are at ~500 eV and originate near the neck region of the Taylor cone since the energy level matches the bias potential. If there is a drop in the energy level of any ion species, then the explanation is that the ions originated at a point further away from the biased emitter, most likely from the jet structure. The energy loss in these ions can be explained by Ohmic losses. As the charged IL extends into the electric field, there is a resultant drop in potential. For a needle emitter, the Taylor cone is much smaller, microscopic in scale, and the needle itself provides a structural element that extends into the Taylor cone. The biased potential is closer to the neck region in a needle than in a capillary. For a capillary, the end of the emitter is blunt and as such the Taylor cone extents from this blunt surface. Instead of just the jet

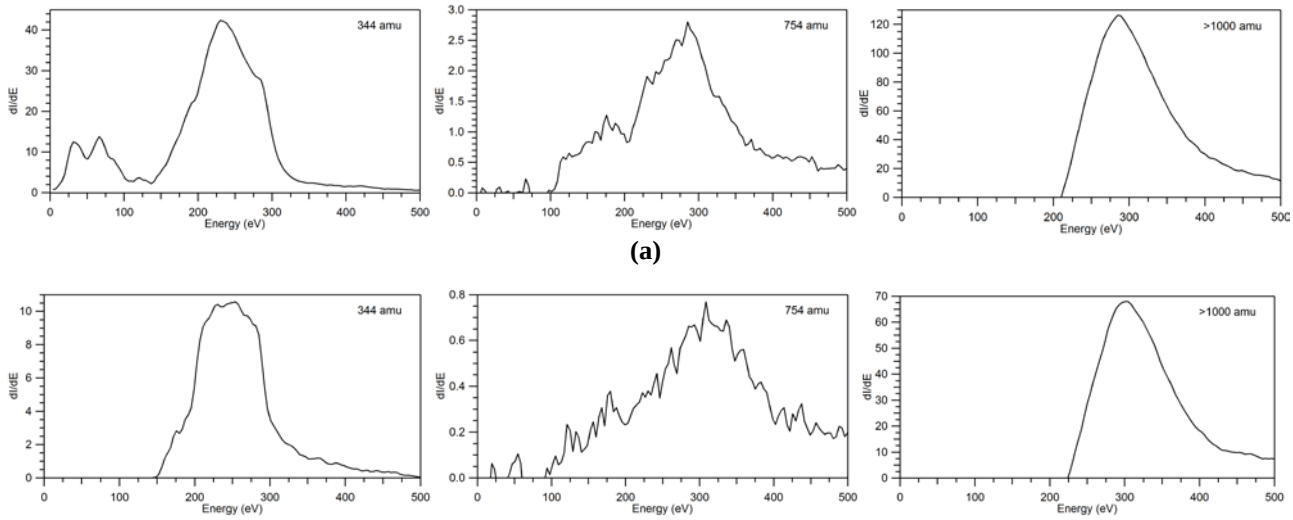

Figure 13. Retarding potential analysis of plume at a IL flow rate of 0.27 nL/s, (a) On-axis (i.e. 0°); (b) Off-axis (i.e. 15°) for 344 amu, 754 amu, and *m/q* > 1000 amu.

undergoing Ohmic losses, the entire Taylor cone of the capillary undergoes Ohmic losses because the entire cone must extend into the electric field. The energy distribution trends show a trail off at high energy levels. This may be an artifact of background levels not detected and perhaps resulting in an offset in the data.

Figure 14 only highlights the 1.24 nL/s energy distributions of 754 amu and *m/q* > 1000 amu since the 344 amu ions occur at trace levels. No significant insight can be gleaned from such low levels. The distribution trends are the same as in the 0.27 nL/s samples. However, the overall energy intensity levels and the energy value at which the peak energy occurs at have dropped. Compared to the mass spectra intensities at 0.27 nL/s, the 1.24 nL/s intensity is lower and as such the 1.24 nL/s energy distributions should be correspondingly lower. The drop in peak energy to less than 300 eV can be explained by the fact that at the 2.2 kV emission voltage, the cone extending from the capillary elongates even further into the electric field when under higher flow rates. This elongation causes further Ohmic losses. The elongation of the cone has been observed through video monitoring of the [Bmim][DCA] cone on the capillary.

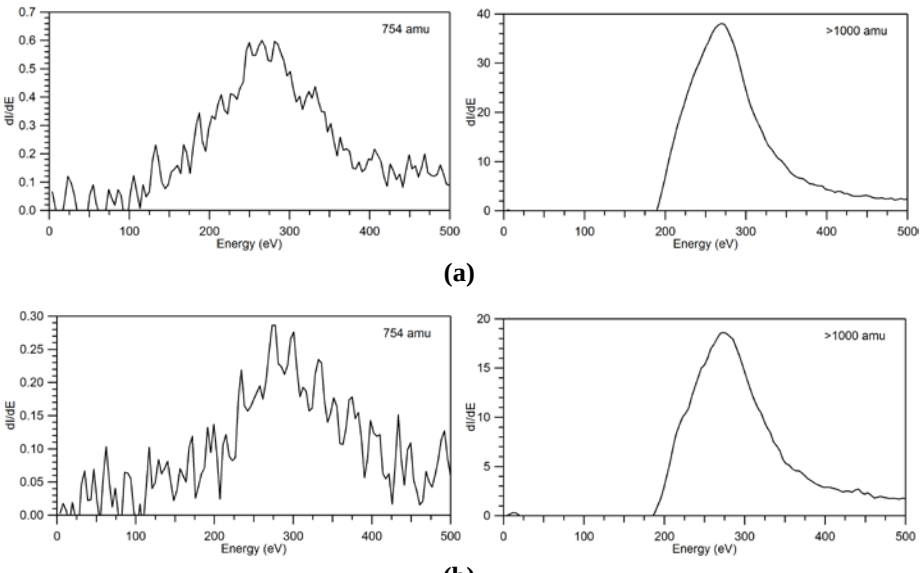

Figure 14. Retarding potential analysis of plume at a IL flow rate of 1.24 nL/s, (a) On-axis; (b) Off-axis for 754 amu, and > 1000 amu.

IV. Conclusion

Angle-resolved current, mass flow rate, ion energy distributions, and mass spectrometric measurements of the IL [Bmim][DCA] are reported. Electrospraying of the IL from both a needle emitter and a capillary emitter under varied flow rate conditions revealed that the electrospray plume underwent operational mode changes corresponding to changes in flow rate. Specifically, the plume broadens in terms of cation mass distribution and current profile as the IL volumetric flow rate increased. The metal needle emitter sprayed in a mixed ion-droplet operation mode, which is typical of needle emitters. Only the n=0,1 species of $Bmim^+([Bmim][DCA])_n$ were significantly emitted over the entire angular range ~ ±30°. Overall the emitted cations were at or closely near a peak energy of ~500 eV (i.e. the needle bias potential) based on the energy distribution scans. Such measurements indicate little Ohmic losses in the beam and that much of the emitted species are emitted near the needle surface.

The capillary emission indicated the most significant changes in the electrospray beam. The current profile initially showed trends and peak current values on the same order of magnitude as the needle emitter. Under increasing flow rates, the current profile broadened to near a reduced, flat line value. Total emission data revealed that at the broadened levels, the spray had widened and much of the plume was missed due to the limited angular range of the experiment. In comparison to the needle data, extremely high mass flow rate values were detected under increasing IL flow rate. The mass flow rate correspondingly showed the same broadening as the current data. The capillary operated at a 0.27 nL/s flow rate revealed a transition in emission profile. The emission profile was a combination of that of a needle and a high flow capillary. All cation species within a *m/q* range of 0-1000 amu (i.e. n=0,1,2,3,4) were observed in the beam. The masses, at the lowest flow rates, were limited to a narrower angular spread of ~ ±20° in comparison to the needle emitter data. With increasing flow rates up to 2.18 nL/s, the cation species within the m/q range almost disappeared from the data. Only the n=2,3,4 were indicated at low intensity levels. The mass distribution changed to reveal a broadening distribution with even intensity levels of the detectable species. The energy distribution of the detected cations showed a clear sign that Ohmic losses had occurred. A peak energy of ~ 300 eV was measured for the cations, which is 200 eV lower than the bias potential. Energy distribution measurements for an $m/q > 1000$ amu showed that at high volumetric flow rates a significant proportion of the beam was associated with larger masses (i.e. large droplets over 1000 amu) unlike needle emitters.

From the [Bmim][DCA] results gathered, there will be trade-offs in electrospray performance depending on emitter style and IL flow rates for any application. Unless at extremely low flow rates where a near ionic-regime composition is achievable, the electrospray plume will include contributions in some proportion from ions less than 1000 amu and large mass droplets. In terms of propulsion application, the volumetric flow rate allows for varied performance from high efficiency I_{SP} to increased thrust levels. This range is on a relative scale applicable to electrospray thrusters. At extremely low flow rates of needle emitter, near ionic-regime to mix ion-droplet operational mode occurs. This flow rate regime will have the best *q/m* ratio and will provide the highest I_{SP} performance. The capillary emission at ~ 0.27 nL/s will be a transitional performance regime resulting in a reduced *q/m* for the gain of mass expulsion (i.e. thrust). Extending to 2.18 nL/s the electrospray beam consists of larger droplets and very few low mass ions. As a result, the beam efficiency will be further reduced. The specific large mass droplets are unknown at this time. Further data are needed to determine the large droplet masses and the role of extraction potential in varying electrospray composition under variable volumetric flow rate conditions.

Acknowledgments

S. W. Miller thanks 1st Lt. Bruce Fritz for conducting retarding energy potential scans of [Bmim][DCA] wetted on a needle emitter. This work was supported by AFOSR task 2303EP02 (Program Manager: Michael Berman).

References

[1]Chiu, Y. and Dressler, R. A., "Ionic Liquids for Space Propulsion," *Ionic Liquids IV: Not Just Solvents Anymore*, American Chemical Society, Washington DC, 2007, p. 138.

[2]Hass, J. M. and Holmes, M. R., "Multi-Mode Propulsion System for the Expansion of Small Satellite Capabilities," 2010, NATO MP-AVT-171-05.

[3]Donius, B. R. and Rovey, J. L., "Ionic Liquid Dual-Mode Spacecraft Propulsion Assessment," *Journal of Spacecraft and Rocket*, Vol. 48, 2011, p. 110.

[4]Donius, B. R., "Investigation of Dual-Mode Spacecraft Propulsion by Means of Ionic Liquids," Masters Thesis, Mechanical and Aerospace Engineering Dept., Missouri University of Science and Technology, Rolla, MO, 2010.

[5]Donius, B. R. and Rovey, J. L., "Analysis and Prediction of Dual-Mode Chemical and Electric Ionic Liquid Propulsion Preformance," *48th Aerospace Sciences Meeting*, Orlando, FL, 2010, AIAA 2010-1328.

[6]Anflo, K., Gronland, T. A., Bergman, G., Johansson, M. and Nedar, R., "Towards Green Propulsion for Spacecraft with ADN-Based Monopropellants," *38th AIAA/ASME/SAE/ASEE Joint Propulsion Conference*, Indianapolis, IN, 2002, AIAA 2002-3847.

[7]Slettenhaar, B., Zevenbergen, J. F., Pasman, H. J., Maree, A. G. M. and Moerel, J. L. P. A., "Study on Catalytic Ignition of HNF Based Non Toxic Monopropellants," *39th AIAA/ASME/SAE/ASEE Joint Propulsion Conference and Exhibit*, Huntsville, AL, 2003, AIAA 2003-4920.

[8]Zube, D. M., Wucherer, E. J. and Reed, B., "Evaluation of HAN-Based Propellant Blends," *39th AIAA/ASME/SAE/ASEE Joint Propulsion Conference & Exhibit*, Huntsville, AL, 2003, AIAA 2003-4643.

[9]Hawkins, T. W., Brand, A. J., McKay, M. B. and Tinnirello, M., "Reduced Toxicity, High Preformance Monopropellant at the U.S. Air Force Research Laboratory," *4th International Association for the Advancement of Space Safety Conference*, Huntsville, AL, 2010.

[10]Romero-Sanz, I., Bocanegra, R., de la Mora, J. F. and Gamero-Castano, M., "Source of heavy molecular ions based on Taylor cones of ionic liquids operating in the pure ion evaporation regime," *Journal of Applied Physics*, Vol. 94, 2003, p. 3599.

[11]Boatz, J. A., Gordon, M. S., Voth, G. A. and Hammes-Schiffer, S., "Design of Energetic Ionic Liquids," *DoD HPCMP Users Group Conference, 2008. DOD HPCMP UGC*, 2008, pp. 196-200.

[12]Smiglak, M., et al., "Combustible ionic liquids by design: is laboratory safety another ionic liquid myth?," *Chemical Communications*, Vol. 2006, p.

[13]Berg, S. P. and Rovey, J. L., "Ignition Evaluation of Monopropellant Blends of HAN and Imidazole-Based Ionic Liquid Fuels," *50th Aerospace Sciences Meeting*, Nashville, TN, 2012, AIAA 2012-0974.

[14]Berg, S. P. and Rovey, J. L., "Dual-Mode Propellant Properties and Performance Analysis of Energetic Ionic Liquids," *50th Aerospace Sciences Meeting*, Nashville, TN, 2012, AIAA 2012-0975.

[15]Amariei, D., Courtheoux, L., Rossignol, S., Batonneau, Y. and Kappenstein, C., "Influence of the Fuel on the Thermal and Catalytic Decompositions of Ionic Liquid Monopropellants," *41st AIAA/SAE/ASEE Joint Propulsion Conference & Exhibit*, Tucson, AZ, 2005, AIAA 2005-3980.

[16]Berg, S. P., "Design and Development of Ionic Liquid Dual-Mode Spacecraft Propellants," Masters Thesis, Mechanical and Aerospace Engineering Dept., Missouri University of Science & Technology, Rolla, MO, 2012.

[17]Fernandez de la Mora, J. and Loscertales, I. G., "The Current Emitted by Highly Conducting Taylor Cones," *Journal of Fluid Mechanics*, Vol. 260, 1994, p. 155.

[18]Gamero-Castaño, M. and Fernandez de la Mora, J., "Direct Measurement of Ion Evaporation Kinetics from Electrified Liquid Surfaces," *Journal of Chemical Physics*, Vol. 113, 2000, p. 815.

[19]Chiu, Y., et al., "Mass Spectrometric Analysis of Ion-Emission from Selected Colloid Thruster Fuels," *39th AIAA/ASME/SAE/ASEE Joint Propulsion Conference and Exhibit*, Huntsville, AL, 2003.

[20]Chiu, Y., Gaeta, G., Levandier, D. J., Dressler, R. A. and Boatz, J. A., "Vacuum Electrospray Ionization Study of the Ionic Liquid, [Emim][Im]," *International Journal of Mass Spectrometry*, Vol. 265, 2007, p. 146.

[21]Lozano, P. C., "Studies on the Ion-Droplet Mixed Regime in Colloid Thrusters," PhD Dissertation, Aeronautics and Astronautics Dept., Massachusetts Institute of Technology, Cambridge, MA, 2003.

[22]Chiu, Y., Gaeta, G., Heine, T. R., Dressler, R. A. and Lavandier, D. J., "Analysis of the Electrospray Plume from the EMI-Im Propellant Externally Wetted on a Tungsten Needle," *42nd AIAA/ASME/SAE/ASEE Joint Propulsion Conference & Exhibit*, Sacramento, CA, 2006.

[23]Ticknor, B. W., Miller, S. W. and Chiu, Y. H., "Mass Spectrometric Analysis of the Electrospray Plume from an Externally Wetted Tungsten Ribbon Emitter," *45th AIAA/ASME/SAE/ASEE Joint Propulsion Confernce & Exhibit*, Denver,CO, 2009, AIAA 2009-5088.

[24]Carvalho, P. J., Regueira, T., Santos, L. M. N. B. F. and Coutinho, J. A. P., "Effect of Water on the Viscosities and Densities of 1-Butyl-3-methylimidazolium Dicyanamide and 1-Butyl-3-methylimidazolium Tricyanomethane at Atmospheric Pressure," Vol. 55, 2010, p. 645.

[25]Sánchez, L. G., Espel, J. R., Onink, F., Meindersma, G. W. and de Haan, A. B., "Density, Viscosity, and Surface Tension of Synthesis Grade Imidazolium, Pyridinium, and Pyrrolidinium Based Room Temperature Ionic Liquids," *Journal of Chemical and Engineering Data*, Vol. 54, 2009, p. 2803.

[26]Ticknor, B. W., Anderson, J. K., Fritz, B. A. and Chiu, Y.-H., "Effect of Aspect Ratio on the Wettability and Electrospray Properties of Porous Tungsten Emitters with the Ionic Liquid [Emim][Im]," *46th AIAA/ASME/SAE/ASEE Joint Propulsion Conference & Exhibit*, Nashville, TN, 2010, AIAA 2010-6618.

[27]Manzella, D. H. and Sankovic, J. M., "Hall Thruster Ion Beam Characterization," *31st AIAA/ASME/ASEE Joint Propulsion Conference and Exhibit*, San Diego, CA, 1995, AIAA 1995-2927.

[28]Chiu, Y., et al., "Mass Spectrometric Analysis of Colloid Thruster Ion Emission from Selected Propellants," *Journal of Propulsion and Power*, Vol. 21, 2005, p. 416.